A Control Strategy based on Fuzzy Logic for Three-phase Grid-connected Photovoltaic System with Supporting Grid-frequency Regulation

Nguyen Gia Minh Thao and Kenko Uchida
Department of Electrical Engineering and Bioscience, Waseda University, Tokyo, Japan
Email: {thao, kuchida}@uchi.elec.waseda.ac.jp

***Abstract*—This paper presents a control strategy based on fuzzy logic to inject efficiently the active power from a three-phase grid-connected photovoltaic (PV) system into the local grid with supporting regulation for the frequency of grid voltage. In which the control strategy consists of three main modules as follows. Firstly, a simulation module based on the mathematical model of a PV panel is utilized to predict the maximum total power from PV arrays; the second one is a frequency regulation module used to compute a proper reference value for the output active power; and the last is a coordinated main controller for power-electronic converters and battery charger to deliver active power to the grid exactly according to the reference value computed beforehand. Especially in the frequency regulation module, a unique fuzzy logic controller (FLC) is designed to help determine accurately the reference value of active power. Besides, a control method for state-of-charge (SOC) of battery bank is also introduced. Simulations show the suggested control strategy has good performances in supplying suitably the active power to grid with regulating the grid frequency in acceptable ranges, even when the solar radiation or AC-system load suddenly changes. Also, effectiveness in regulating grid frequency of the proposed control strategy is compared with the conventional strategy using full maximum power point tracking (MPPT) mode.**

***Index Terms*—grid-connected PV system, grid-frequency regulation, coordinated control, battery state-of-charge control, fuzzy logic, MPPT, multi-string PV array, per-unit**

I. Introduction

Recently, for environmental preservation purpose, grid-connected PV systems have been widely utilized to deliver active power to the electric grid. However, many grid-connected PV systems integrated in the local grid may cause the frequency deviation of grid voltage to exceed much over the acceptable range of ±0.2 *Hz*. So the grid-frequency regulation issue in a local grid with high penetration grid-connected PV systems should be considered to resolve thoroughly. In fact, this is currently an interesting research theme for many scholars [1]-[9].

In [2]-[5], a coordinated control based on fuzzy logic for PV-diesel hybrid systems without the battery bank has been introduced to regulate the grid frequency. This strategy used two 49-rule fuzzy logic controllers (FLCs) to determine the reference value for active power needed to inject into the grid. Besides, according to [6, 7], grid-connected PV systems with the battery bank have been utilized to regulate the grid frequency. Nevertheless, the common drawback of most these studies is that the state-of-charge (SOC) of battery bank has not been regulated in the safe range of [0.2 0.8] to ensure durability of battery.

On the other hand, a grid frequency control technique based on power curtailment using the Newton quadratic interpolation (NQI) for the PV grid-connected system without energy storage has been presented in [8]. The technique utilizes fairly many calculation steps to force PV arrays to operate exactly according to the reference power value. This may reduce the response speed of the technique. Referring in [9], a double-layer capacitor and a proportional controller for grid-connected PV system have been used to regulate grid frequency. The control method has not only the pretty simple structure but also good performances. However, effects of AC-system load in the grid have not yet been considered in the study.

Motivated by the above observation, in this paper, the proposed control strategy for three-phase grid-connected PV system with a battery bank to support grid-frequency regulation has three main objectives as follows.

i. The output active power from the PV system delivered to the grid is adjusted suitably to ensure the grid frequency in tolerable ranges. In this study, two acceptable ranges for frequency deviation are ±0.2 *Hz* in transient state and ±0.1 *Hz* at steady state, where the nominal grid frequency is 60 *Hz*.
ii. As well, SOC of battery bank is always kept in the safe range of [0.2 0.8] to ensure durability of the battery bank. Moreover, at the steady state, SOC of battery bank is regulated to the value of 0.5.
iii. The grid-frequency deviation is also controlled to be always in the tolerable ranges above in both the transient state and steady state even if the solar radiation or AC-system load unexpectedly fluctuates.

To fulfill the goals listed above, the proposed control strategy is designed with three major modules. In detail, the first module uses the mathematical model of PV panel, measured values of solar radiation and air temperature to predict relatively the maximum total power of four PV arrays; then, the second one uses the measured value of

Manuscript received July 1, 2014; revised May 11, 2015.

doi: 10.12720/joace.4.2.96-103

grid frequency and the predicted total energy capacity of the PV arrays and battery bank to determine a suitable reference value for the output active power; and finally, the third module coordinately controls all the power-electronic converters and battery charger to inject the active power into the grid exactly according to the desired value computed beforehand by the second module. Especially, in the suggested strategy of this study, a new FLC is developed to implement into the second module, and a unique control algorithm used for regulating SOC of battery bank is also proposed in the third module.

II. Demonstrative Grid-connected PV System with Multi-String PV Array Topology

A. System Description

The demonstrative grid-connected PV system and the proposed control strategy are shown in Fig. 1. Wherein, there are four strings of PV arrays where each string has the nominal power of 2.5*kW*. And the DC-DC converter used for each 2.5*kW* PV string can be chosen as the non-inverting buck-boost converter as presented in [10, 11]. The battery bank can supply or absorb power via the bidirectional charger based on a half-bridge buck-book converter [6, 7]. Then, output power is delivered to the three-phase AC bus via a DC-AC inverter. For study about the grid-frequency deviation, the local grid can be modeled as a synchronous generator, including the speed governor as shown in Fig. 2 and [3, 4, 8], and a system AC-system load is connected to the three-phase AC bus.

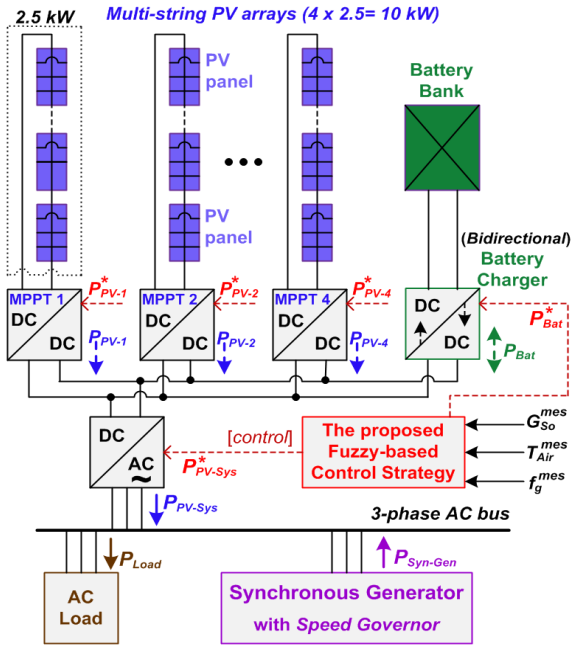

Figure 1. The demonstrative grid-connected PV system in this study

From the measured values of solar radiation, air temperature, grid frequency and SOC of battery bank, the proposed fuzzy-based strategy will generate the control signals (labeled with the asterisk) for the four DC-DC converters connected with PV strings, the bidirectional DC-DC battery charger and the DC-AC inverter.

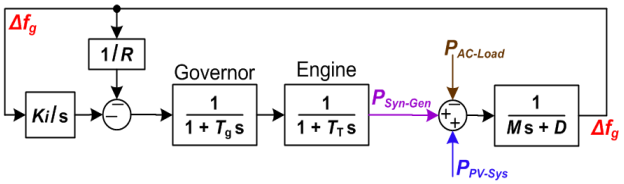

Figure 2. The diagram of speed governor for synchronous generator

According to [12], [13], the multi-string PV converter topology has advantages as: high-energy yield because of separate MPPT algorithm, installment cost reduction, optimal monitoring of PV system and much compatibility for large-scale PV grid-connected systems. Indeed, commercial products based on the multi-string converter topology for PV system have been introduced fairly popular. In this study, the multi-string converter topology is applied in the illustrative PV system as shown in Fig. 1.

B. PV Panel Model

According to [1, 10], the one-diode equivalent model of a PV panel is expressed in Fig. 3 and (1).

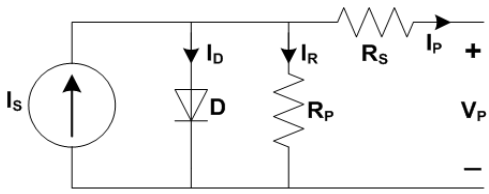

Figure 3. The equivalent circuit for a PV panel.

$$I_P = N_P I_S - N_P I_O \left[\mathrm{e}\left(\frac{q\left(V_P + R_S I_P\right)}{N_S a k T_{Cell}} \right) - 1 \right] - N_P \left(\frac{V_P + R_S I_P}{N_S R_P} \right) \quad (1)$$

$$I_S\left(T_{Cell}, G_{So}\right) = \left[I_{SC,n} + k_T \left(T_{Cell} - T_n \right) \right] \frac{G_{So}}{G_n} \quad (2)$$

$$I_O(T_{Cell}) = \left[\frac{I_{SC,n}}{\mathrm{e}\left(\frac{qV_{OC,n}}{N_S a k T_{Cell}} \right) - 1} \right] \left(\frac{T_{Cell}}{T_n} \right)^3 \mathrm{e}\left[\frac{qE_g}{ak} \left(\frac{1}{T_n} - \frac{1}{T_{Cell}} \right) \right] \quad (3)$$

I_S is the photoelectric current related to the solar radiation; I_O is the saturation diode current; $I_{SC,n}$ and $V_{OC,n}$ are the short-circuit current and the open-circuit voltage of the PV panel at the nominal condition, respectively; q is the electric charge, 1.602×10^{-19}; a is the diode ideality constant and its value is in the interval [1 2]; k is the Boltzmann's constant, 1.381×10^{-23} (J/K); E_g is the energy gap of the material used to make the solar cell, 1.12 (eV); k_T is the temperature coefficient, 0.075 (%/K); N_S and N_P are the number of solar cells in series and parallel respectively in the PV panel; G_{So} and G_n = 1000 (W/m^2), are the solar irradiance at the operating condition and nominal condition, respectively; T_{Cell} and T_n = 298 (K), are the absolute temperatures of the solar cell at the operating condition and nominal condition, respectively.

III. The Proposed Fuzzy-Based Control Strategy

The structure of the proposed fuzzy-based strategy is illustrated in Fig. 4. Wherein, the coordinated main controller uses the predicted maximum power value from PV arrays simulated by the prediction module and the measured SOC of the battery bank to calculate the maximum total power capacity. Meanwhile, the proposed FLC determines the adjustable value $\Delta\beta^{pre}(k)$ for updating the reference value for active power $\beta^{*}(k)$ from the desired value and measured value of grid frequency. Then, the active-power reference value needed to inject into the grid will be computed according to (9) and (10). Finally, the coordinated controller module controls suitably the DC-DC converter at each PV string, bidirectional DC-DC battery charger and three-phase DC-AC inverter to deliver the output power according to the reference value.

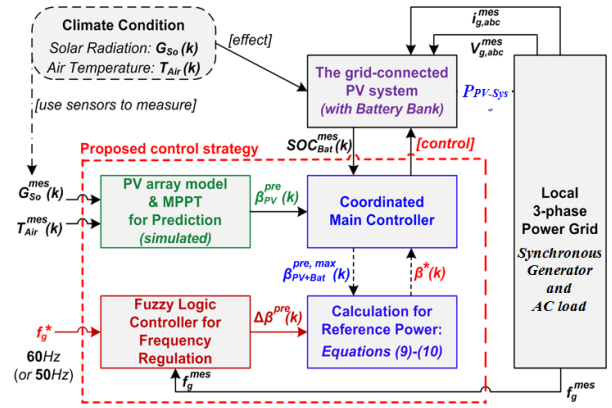

Figure 4. Structure of the proposed control strategy with three modules

A. The Prediction Module (The First Module)

The detailed structure of the prediction module (the first module of the proposed control strategy) is presented in Fig. 5. Wherein, the mathematical model of each PV panel is based on (1)-(3), and the manufacturing parameter values of PV panel are provided by Table I.

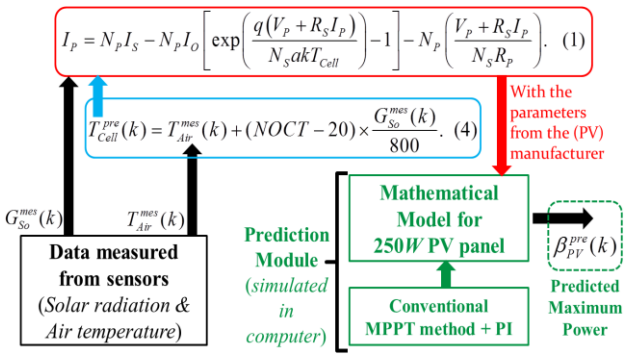

Figure 5. The detailed scheme of the prediction module

According to [14], [15], using the Nominal Operating Cell Temperature (NOCT) coefficient, the temperature of PV cell (inside PV panel) can be estimated from the measured value of air temperature as follows:

$$T_{Cell}^{pre}(k) = T_{Air}^{mes}(k) + (NOCT - 20) \times \frac{G_{So}^{mes}(k)}{800} \quad (4)$$

From the measured value of solar radiation using sensor and the PV cell temperature estimated in (4), the output current of each PV panel can be computed by (1). Then, Fig. 6 is modeled and implemented in computer simulation to predict the maximum power of a PV panel. Wherein, the mathematical model of non-inverting buck-boost converter and the conventional MPPT method with PI controller can be found in [10, 1]. Lastly, the predicted maximum total power of all PV arrays will be computed and sent to the coordinated main controller (the third module of proposed strategy) as shown in Fig. 4 and Fig. 5.

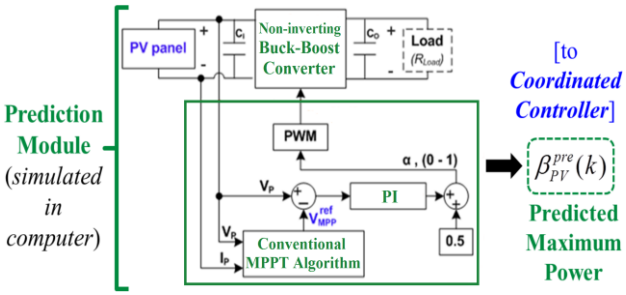

Figure 6. Structure for implementing MPPT algorithm for PV panel

TABLE I. Nominal Parameter Values of the 250W PV Panel

Parameter	Symbol	Value
Maximum output power (nominal)	P_P^{max}	250 W
Voltage at the MPP	V_{MPP}	30.4 V
Current at the MPP	I_{MPP}	8.23 A
Open-circuit voltage	V_{OC}	38.1 V
Short-circuit current	I_{SC}	8.91 A
Number of cells in series, parallel	N_S , N_P	60 , 1
Number of PV panels of each PV array (each string) in Fig. 1	$N_{PV\text{-}panels}$	10 (10 x 250W = 2.5 kW /array)

B. Design Steps of the Coordinated Main Controller with Regulating SOC of Battery Bank (The Third Module)

Step 1: Firstly, all parameters are converted to per-unit (p.u) values to simply the design process of the proposed strategy [16]. Per-unit values labeled as β are given in (5).

$$\begin{cases} P_{PV}^{rated} = 10kW;\ \beta_{Bat}^{rated} = \dfrac{P_{Bat}^{rated}}{P_{PV}^{rated}} = 0.8 \\ \beta_{PV}^{pre}(k) = \dfrac{P_{PV}^{pre}(k)}{P_{PV}^{rated}};\ \beta^{*}(k) = \dfrac{P_{PV-Sys}^{*}(k)}{P_{PV}^{rated}} \end{cases} \quad (5)$$

Step 2: The power supply and absorption capacity of the battery bank is calculated by (6) and (7), respectively.

$$\beta_{Bat}^{pre,\,supply}(k) = \begin{cases} 0\ , \text{if}\ \ SOC_{Bat}^{mes}(k) < SOC_{Bat}^{min} = 0.2 \\ \left[SOC_{Bat}^{mes}(k) - SOC_{Bat}^{min}\right] \times \beta_{Bat}^{rated}\ , \text{if else} \end{cases} \quad (6)$$

$$\beta_{Bat}^{pre,\ \text{absorb}}(k)=\begin{cases}0\ , \text{if}\ \ SOC_{Bat}^{mes}(k)>SOC_{Bat}^{\max}=0.8\\ \left[SOC_{Bat}^{mes}(k)-SOC_{Bat}^{\max}\right]\times\beta_{Bat}^{rated}\ , \text{if else}\end{cases} \quad (7)$$

The predicted maximum total power capacity of the four PV arrays and battery bank is expressed as (8).

$$\beta_{PV+Bat}^{pre,\max}(k)=\beta_{PV}^{pre}(k)+\beta_{Bat}^{pre,\ \text{supply}}(k) \quad (8)$$

$$\beta_{PV-Sys}^{mes}(k-1)=\beta_{PV}^{mes}(k-1)+\beta_{Bat}^{mes}(k-1) \quad (9)$$

With the adjustable value $\Delta\beta^{pre}(k)$ from Fig. 4 and Fig. 7, the k th reference value for active power is updated by

$$\beta^{*}(k)=\beta_{PV-Sys}^{mes}(k-1)\ +\ \Delta\beta^{pre}(k) \quad (10)$$

where its limitation is $0\le\ \beta^{*}(k)\ \le\beta_{PV+Bat}^{pre,\max}(k)$.

Step 3: To determine the operation mode for each DC-DC converter, a ratio value $\delta(k)$ is defined as follows:

$$\delta(k)\ =\ \left[\frac{\beta^{*}(k)}{\beta_{PV}^{pre}(k)}\right]\times100\% \quad (11)$$

In this study, it is noted that PV strings are installed in a not too-large area, so the predicted maximum power of each PV string can be assumed to be equivalent together.

a. If $\delta(k)\ge100\%$: All the DC-DC converters for PV arrays will be controlled to operate with MPPT mode.

b. If $75\%\le\ \delta(k)<100\%$, we check two sub-cases:
If $SOC_{Bat}^{mes}(k)<SOC_{Bat}^{\max}$: all the four DC-DC converters for PV arrays will be controlled to operate with MPPT mode; meanwhile, the battery bank will be predicted to absorb power.
If $SOC_{Bat}^{mes}(k)\ \ge\ SOC_{Bat}^{\max}$: the three DC-DC converters for the 1st, 2nd and 3rd PV arrays will be controlled to operate with MPPT mode; meanwhile, the 4th DC-DC converter will be deactivated, and the battery bank will be predicted to supply power.

c. If $50\%\ \le\ \delta(k)<75\%$, we check two sub-cases:
If $SOC_{Bat}^{mes}(k)<SOC_{Bat}^{\max}$: the three DC-DC converters for the 1st, 2nd and 3rd PV arrays will be controlled to operate with MPPT mode; meanwhile, the 4th DC-DC converter will be deactivated, and the battery bank will be predicted to absorb power.
If $SOC_{Bat}^{mes}(k)\ \ge\ SOC_{Bat}^{\max}$: the two DC-DC converters for the 1st and 2nd PV arrays will be controlled to operate with MPPT mode; meanwhile, the 3rd and 4th DC-DC converters will be deactivated, and the battery bank will be predicted to supply power.

d. If $25\%\ \le\ \delta(k)<50\%$, we check two sub-cases:
If $SOC_{Bat}^{mes}(k)<SOC_{Bat}^{\max}$: the two DC-DC converters for the 1st and 2nd PV arrays will be controlled to operate with MPPT mode; meanwhile, the 3rd and 4th DC-DC converters will be deactivated, and the battery bank will be predicted to absorb power.
If $SOC_{Bat}^{mes}(k)\ \ge\ SOC_{Bat}^{\max}$: the DC-DC converter for the 1st PV array will be controlled to operate with MPPT mode; meanwhile, the 2nd, 3rd and 4th DC-DC converters will be deactivated, and the battery bank will be predicted to supply power.

e. Else ($0\%\ \le\ \delta(k)<25\%$), we check two sub-cases:
If $SOC_{Bat}^{mes}(k)<SOC_{Bat}^{\max}$: the DC-DC converter for the 1st PV array will be controlled to operate with MPPT mode; meanwhile, the 2nd, 3rd and 4th DC-DC converters will be deactivated, and the battery bank will be predicted to absorb power.
If $SOC_{Bat}^{mes}(k)\ \ge\ SOC_{Bat}^{\max}$: All the four DC-DC converters for PV arrays will be deactivated, and the battery bank will be predicted to supply power.

Step 4: Measure the kth real total operating power of all PV arrays $\beta_{PV}^{mes}(k)$, and then compute the value $\beta_{SUB}(k)$.

$$\beta_{SUB}(k)=\beta^{*}(k)\ -\ \beta_{PV}^{mes}(k) \quad (12)$$

Step 5: Determine the amount of active power should be supplied or absorbed from battery bank and the operation mode (supplying or absorbing) for the battery bank. The detailed algorithm is given as below.

a. If $\beta^{*}(k)<\beta_{PV}^{mes}(k)$, we check two sub-cases:
If $SOC_{Bat}^{mes}(k)<SOC_{Bat}^{\max}=0.8$: the battery bank can continue to absorb power; therefore, it will be controlled to absorb power according to the reference value for battery bank as follows.

$$\beta_{Bat}^{*}(k)=\beta_{SUB}(k)<0 \quad (13)$$

However, if $\beta_{SUB}(k)<\beta_{Bat}^{pre,\ absorb}(k)$, we reset as

$$\beta_{Bat}^{*}(k)=\beta_{Bat}^{pre,\ absorb}(k) \quad (14)$$

Else ($SOC_{Bat}^{mes}(k)\ge SOC_{Bat}^{\max}$): The battery bank cannot absorb any further power. So, in this case, the battery bank will be controlled to operate in the neutral mode: $\beta_{Bat}^{*}(k)=0$.

b. If $\beta^{*}(k)\ \ge\ \beta_{PV}^{mes}(k)$, we check two sub-cases:
If $SOC_{Bat}^{mes}(k)\ \le\ SOC_{Bat}^{\min}=0.2$, the battery bank cannot supply power any more. Thus, in this condition, the battery bank will be controlled to operate in the neutral mode: $\beta_{Bat}^{*}(k)=0$.
Else ($SOC_{Bat}^{mes}(k)>SOC_{Bat}^{\min}$): the battery bank will be controlled to supply power.

$$\beta_{Bat}^{*}(k)=\beta_{SUB}(k)>0 \quad (15)$$

However, if $\beta_{SUB}(k)>\beta_{Bat}^{pre,\ \text{supply}}(k)$, we reset as

$$\beta_{Bat}^{*}(k)=\beta_{Bat}^{pre,\ \text{supply}}(k) \quad (16)$$

Step 6: At the steady state, if the frequency deviation is in the range of [-0.075 0.075], the battery bank will be priorly controlled to regulate its SOC to the value of 0.5. The purpose of this step is to ensure the battery bank can absorb/supply sufficiently energy as needed for next

operation time. The detailed algorithm for regulating SOC of battery bank is presented as below.

If $\left|Ef_g(k)\right| \le 0.075$, we check three sub-cases:

If $SOC_{Bat}^{mes}(k) < 0.5$: The battery DC-DC charger will be controlled to absorb power from PV arrays to force SOC of the battery bank reach the value of 0.5.

If $SOC_{Bat}^{mes}(k) > 0.5$: The battery DC-DC charger will be controlled to inject power into the grid via the DC-AC inverter to decrease SOC of the battery bank to the desired value of 0.5.

Else ($SOC_{Bat}^{mes}(k) = 0.5$): The battery bank will be kept to operate in the neutral (rest) mode.

C. *Design Structure of the Proposed FLC Used in the Frequency Regulation Module (The Second Module)*

As shown in Fig. 7, the proposed FLC uses the error of grid frequency $Ef_g(k)$ (this value is also the frequency deviation Δf_g in Fig. 2) and its derivative $dEf_g(k)$ as two inputs to determine the adjustable value $\Delta\beta^{pre}(k)$. Then, $\Delta\beta^{pre}(k)$ will be utilized to update suitably the reference value for active power $\beta^{*}(k)$ as expressed in (10).

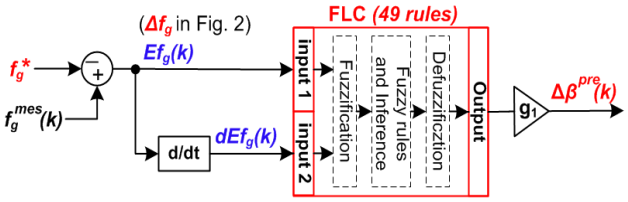

Figure 7. Design structure of the proposed FLC in the second module

Two Inputs:

The first input has seven linguistic variables and value in the interval of [-0.3 0.3].

$Ef_g(k)$ = {Negative Large, Negative Medium, Negative Small, Zero, Positive Small, Positive Medium, Positive Large}
= [NL, NM, NS, ZE, PS, PM, PL]

The second input has seven linguistic variables and value in the interval of [-0.3 0.3].

$dEf_g(k)$ = {Negative Large, Negative Medium, Negative Small, Zero, Positive Small, Positive Medium, Positive Large}
= [NL, NM, NS, ZE, PS, PM, PL]

The Output: has nine linguistic variables and value in the interval of [-0.4 0.4]

$\Delta\beta^{pre}(k)$ = {Negative Ultimate, Negative Large, Negative Medium, Negative Small, Zero, Positive Small, Positive Medium, Positive Large, Positive Ultimate}
= [NU, NL, NM, NS, ZE, PS, PM, PL, PU]

Membership Functions:

The membership functions for the two inputs and output of the proposed FLC are described in Fig. 8, Fig. 9 and Fig. 10, respectively.

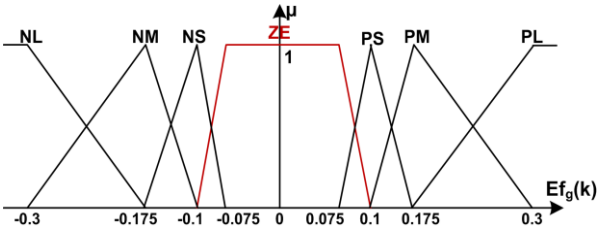

Figure 8. The membership functions for the first FLC's input.

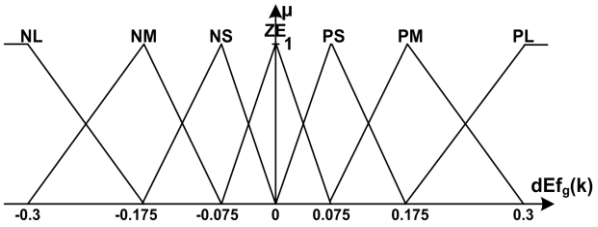

Figure 9. The membership functions for the second FLC's input.

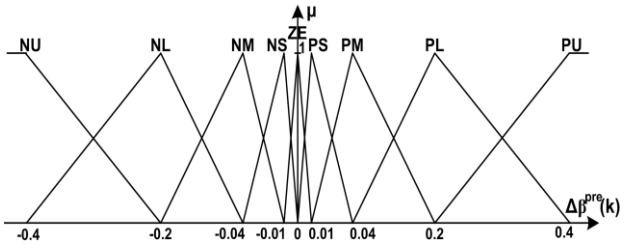

Figure 10. The membership functions for the first FLC's output.

The fuzzy associative matrix is described in Table II. It has totally $7 \times 7 = 49$ rules, and each rule is represented in the form "**if**…**then**…". A sample rule is expressed as "**if** $Ef_g(k)$ is NL and $dEf_g(k)$ is PL **then** $\Delta\beta^{pre}(k)$ is ZE".

TABLE II. FUZZY ASSOCIATION RULES OF THE PROPOSED FLC

$\Delta\beta^{pre}(k)$		$Ef_g(k)$						
		NL	NM	NS	ZE	PS	PM	PL
$dEf_g(k)$	NL	PU	PU	PL	PM	PM	PS	ZE
	NM	PU	PL	PL	PM	PS	ZE	NS
	NS	PL	PL	PM	PS	ZE	NS	NM
	ZE	PL	PM	PS	ZE	NS	NM	NL
	PS	PM	PS	ZE	ZE	NM	NL	NL
	PM	PS	ZE	NS	ZE	NL	NL	NU
	PL	ZE	NS	NM	NS	NL	NU	NU

The fuzzy rules are developed according to the authors' logical deduction based on experiences about the grid-connected PV systems, including the battery bank. Additionally, in this paper, the fuzzy association rules have been also checked with the trial-and-error method.

IV. SIMULATION RESULTS

Values for parameters of the demonstrative PV system with the proposed control strategy in Matlab simulation [17] are shown in Table III. Besides, the conventional strategy based on full MPPT mode for the PV system will be also simulated to evaluate efficacy of the suggested

fuzzy-based strategy. It is noted that, in the conventional strategy based on full MPPT mode, all the power obtained from PV arrays is delivered to the grid.

TABLE III. PARAMETER VALUES USED IN MATLAB SIMULATION

Parameter values of the speed governor (in Fig. 2):
K_i = 9.5 ; R = 0.1 ; T_g = 0.2 ; T_T = 0.5 ; M = 4 ; K_i = 0.4
Parameter values of the proposed FLC (in Fig. 7):
g_1 = 0.35 ; max-min fuzzy inference ; centroid defuzzification
Sampling time for generating control signal: $T_{s\_control}$ = 0.05*s*

A. *Case 1: AC-System Load is Decreased of 40% at the Time t = 22 s, and Solar Radiation is Constant*

Results obtained for this case are illustrated in Fig. 11, including the three sub-parts (a), (b) and (c). In detail, according to Fig. 11(a), the frequency deviation with the proposed control strategy (the red-color solid line) is always much smaller than the other ones. In fact, it is regulated strictly in range of ±0.2 *Hz* in transient states and also in range of ±0.1 *Hz* at steady states. Meanwhile, the frequency with the conventional strategy with full MPPT mode (the blue-color dash line) exceeds the lower limitation of -0.2 *Hz* in the time period t = [0.4*s* 1.2*s*] and has pretty large oscillation at the steady states. Lastly, if without the energy compensation provided by the grid-connected PV system, the frequency deviation (the black-color dash-dot line) becomes to be very large.

Moreover, as shown in Fig. 11(b), the actual total active power injected into the grid is controlled exactly according to the reference value computed in advance by the proposed control strategy. Besides, the battery bank is controlled to supply power in about the two periods *t* = [0*s* 2*s*] and *t* = [23.5*s* 28*s*], and to absorb energy in about the two periods *t* = [2*s* 5*s*] and *t* = [22.3*s* 23.5*s*] (when the AC-system load is unexpectedly decreased of 40%) as illustrated in Fig. 11(c). The proper operation of battery bank using the proposed control strategy actually helps reduce efficiently the grid-frequency deviation.

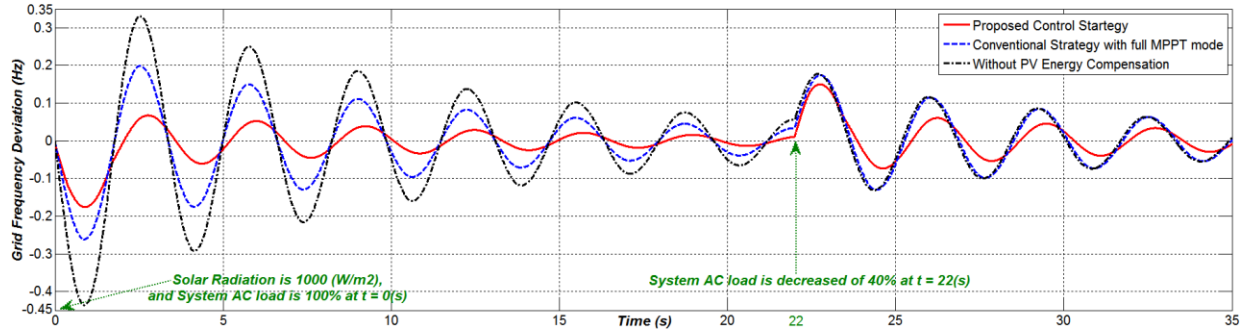

(a) Grid frequency deviation in *Case 1*

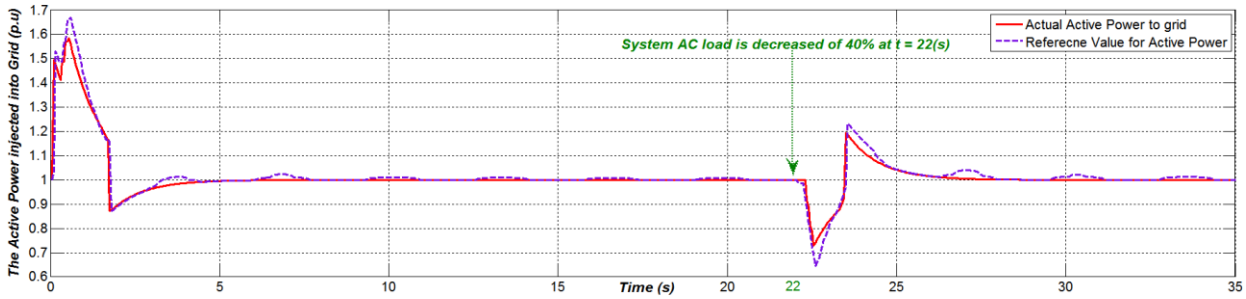

(b) Active power injected into grid with the proposed fuzzy-based control strategy in *Case 1*

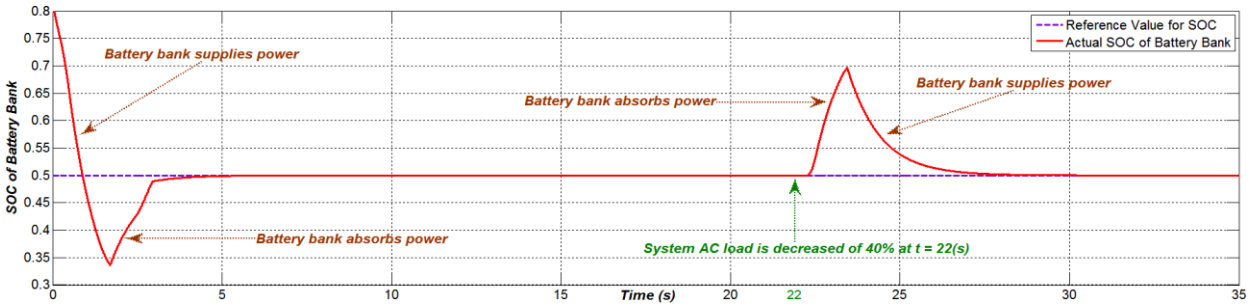

(c) SOC of the battery bank with the proposed fuzzy-based control strategy in *Case 1*

Figure 11. Simulation results in *Case 1* where the AC-system load is decreased suddenly of 40% at the time *t* = 22 (s)

B. *Case 2: Solar Radiation Decreases of 40% at the Time t = 22 s, and AC-System Load is Invariant*

In this operation condition, results are illustrated in Fig. 12, including three sub-parts (a), (b) and (c). In detail, as presented in Fig. 12(a), the frequency deviation with the proposed control strategy (the red-color solid line) is always fairly much smaller than the other response with the conventional strategy using full MPPT mode (the blue-color dash line). Obviously, the response with the proposed control strategy has satisfied well for all the

listed requirements for grid-frequency regulation.

Furthermore, as illustrated in Fig. 12(b), the actual active power of PV system supplied to the grid is almost equal to the reference value determined beforehand by the suggested strategy. As well, the battery bank is also controlled suitably to supply active power in about the two periods t = [0s 2s] and t = [22.3s 23.5s] (when the solar radiation decreases of 40%), and to absorb power in about two periods t = [2s 5s] and t = [23.5s 28s], as seen in Fig. 12(c). Besides, SOC of battery bank is always kept in the safe range of [0.2 0.8] in all the operation time, and is maintained at the desired value of 0.5 at steady states.

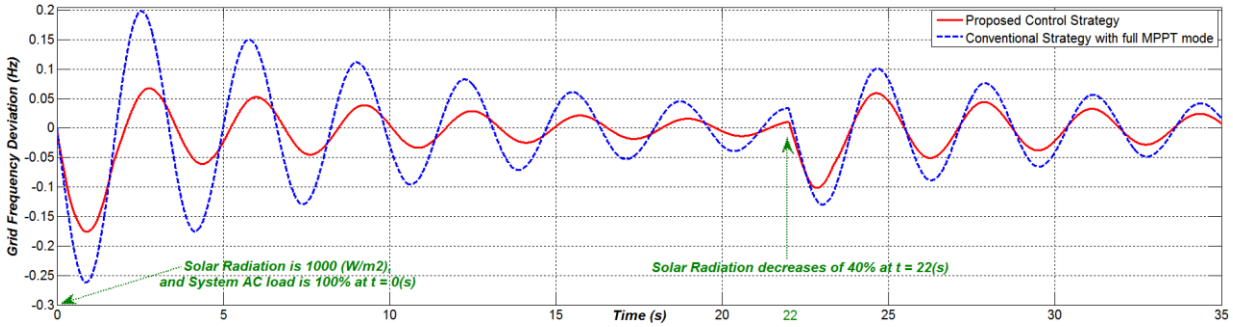

(a) Grid frequency deviation in *Case 2*

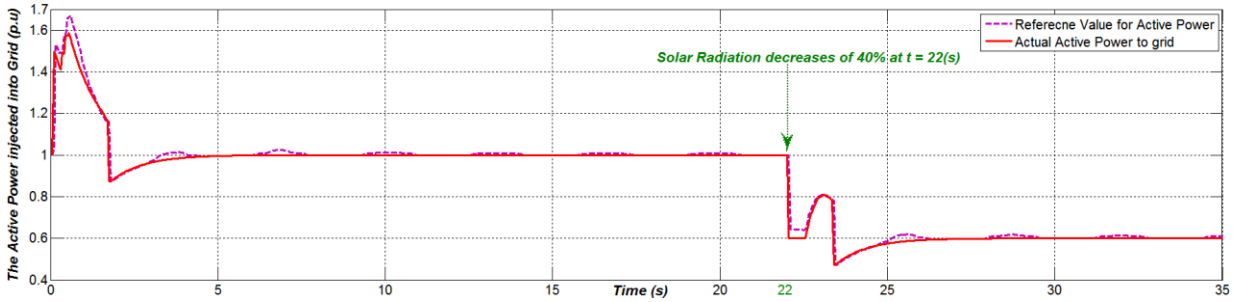

(b) Active power injected into grid with the proposed fuzzy-based control strategy in *Case 2*

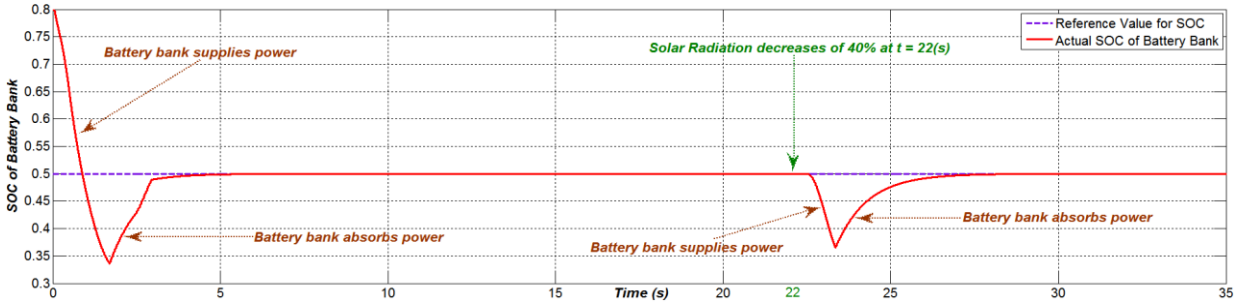

(c) SOC of the battery bank with the proposed fuzzy-based control strategy in *Case 2*

Figure 12. Simulation results in *Case 2* where the solar radiation decreases abruptly of 40% at the time t = 22 (s)

V. Conclusion

This paper has presented a fuzzy-based control strategy with supporting grid-frequency regulation for a three-phase grid-connected PV system, including battery bank. In detail, the control strategy consists of a frequency-regulation module using a newly designed FLC to determine the suitable reference value for the active power; and then controls coordinately the four DC-DC converters, bidirectional DC-DC battery charger and DC-AC inverter to deliver the output active power to grid for forcing the grid-frequency into the acceptable range of ±0.2 *Hz* in transient states and especially in the range of ±0.1 *Hz* at steady states. Simulations have shown the advantages of the proposed control strategy not only in injecting active power into the grid but also in regulating the grid frequency, as well as keeping SOC of the battery bank to be in the safe range of [0.2 0.8] in all operation time and close to the value of 0.5 at the steady state.

Furthermore, comparisons in simulation results, obtained with the suggested control strategy, the conventional strategy based on full MPPT mode and another operation strategy without the PV power, has also demonstrated clearly effectiveness of the presented fuzzy-based strategy, especially when the solar radiation or AC-system load varies abruptly and significantly.

In our next study, the designed method based on fuzzy logic for the frequency regulation module will be improved to boost significantly the efficacy. As well, an efficient control strategy for the megawatt-class PV energy farm, consisting of many 10*kW* three-phase grid-connected PV systems, will be also developed.

ACKNOWLEDGMENT

This work was partially supported by JST-CREST.

REFERENCES

[1] B. N. Alajmi, K. H. Ahmed, S. J. Finney, and B. W. Williams, "Fuzzy-logic control approach of a modified hill-climbing method for maximum power point in microgrid standalone pv system," *IEEE Transaction on Power Electronics*, vol. 26, no. 4, pp. 1022-1030, 2011.

[2] M. Datta, T. Senjyu, A. Yona, H. Sekine, and T. Funabashi, "Smoothing output power variations of isolated utility connected multiple pv systems by coordinated control," *Journal of Power Electronics*, vol. 9, no. 2, pp. 320-333, March 2009.

[3] M. Datta, T. Senjyu, A. Yona, T. Funabashi, and C. H. Kim, "A coordinated control method for leveling pv output power fluctuations of pv–diesel hybrid systems connected to isolated power utility," *IEEE Transactions on Energy Conversion*, vol. 24, no. 1, pp. 153-162, March 2009.

[4] M. Datta, T. Senjyu, A. Yona, T. Funabashi, and C. H. Kim, "A frequency-control approach by photovoltaic generator in a pv–diesel hybrid power system," *IEEE Transactions on Energy Conversion*, vol. 26, no. 2, pp. 559-571, June 2011.

[5] M. Datta, H. Ishikawa, H. Naitoh, and T. Senjyu, "LFC by coordinated virtual inertia mimicking and pevs in power utility with mw-class distributed pv generation," in *Proc. IEEE 13th Workshop on COMPEL 2012*, Invited Presentation, Japan, June 2012.

[6] M. Datta, T. Senjyu, A. Yona, T. Funabashi, and C. H. Kim, "Fuzzy control of distributed pv inverters/energy storage systems/electric vehicles for frequency regulation in a large power system," *IEEE Transactions on Smart Grid*, vol. 4, no. 1, pp. 479-488, March 2013.

[7] K. Sun, L. Zhang, Y. Xing, and J. M. Guerrero, "A distributed control strategy based on dc bus signaling for modular photovoltaic generation systems with battery energy storage," *IEEE Transactions on Power Electronics*, vol. 26, no. 10, pp. 3032-3045, October 2011.

[8] H. Xin, Y. Liu, Z. Wang, D. Gan, and T. Yang, "A new frequency regulation strategy for photovoltaic systems without energy storage," *IEEE Transactions on Sustainable Energy*, vol. 4, no. 4, pp. 985-993, October 2013.

[9] N. Kakimoto, S. Takayama, H. Satoh, and K. Nakamura, "Power modulation of photovoltaic generator for frequency control of power system," *IEEE Transactions on Energy Conversion*, vol. 24, no. 4, pp. 943-949, December 2009.

[10] N. G. M. Thao and K. Uchida, "Control the photovoltaic grid-connected system using fuzzy logic and backstepping approach," in *Proc. IEEE 9th Asian Control Conference*, Istanbul, Turkey, June 2013, pp. 1-8.

[11] H. Sira-Ram ́ırez and R. Silva-Ortigoza, Control Design Techniques in Power Electronics Devices, *Springer*, December 2010.

[12] M. Meinhardt, G. Cramer, B. Burger, and P. Zacharias, "Multi-string-converter with reduced specific costs and enhanced functionality," *Solar Energy*, Supplement 6, vol. 69, pp. 217–227, July–December 2001.

[13] D. C. Martins, "Analysis of a three-phase grid-connected pv power system using a modified dual-state inverter," *ISRN Renewable Energy*, vol. 2013, pp. 18.

[14] E. Skoplaki and J. A. Palyvos, "On the temperature dependence of photovoltaic module electrical performance: A review of efficiency/power correlations," *Solar Energy*, vol. 83, pp. 614–624, 2009.

[15] M. C. Garcia and J. L. Balenzategui, "Estimation of photovoltaic module yearly temperature and performance based on nominal operation cell temperature calculations," *Renewable Energy*, vol. 29, pp. 1997–2010, 2004.

[16] N. G. M. Thao and K. Uchida, "Active and reactive power control techniques based on feedback linearization and fuzzy logic for three-phase grid-connected photovoltaic inverters," *Asian Journal of Control*, vol. 17, no. 5, pp. 1-25, September 2014.

[17] A. Notholt, D. Coll-Mayor, and A. Engler, "Setting up a grid simulator," in *Proc. International Conference on Power Quality and Renewable Energies*, Palma de Mallorca, April 5-7, 2006.

Nguyen Gia Minh Thao obtained his B.Eng. and M.Eng. degrees of Electrical-Electronics Engineering from Ho Chi Minh City University of Technology (HCMUT), Vietnam, in 2009 and 2011, respectively. Since April 2009, he became a probationary lecturer at Faculty of Electrical and Electronics Engineering, HCMUT, where he has been a Lecturer since January 2012. He is currently a PhD student at Waseda University, Japan. His research interests include nonlinear control, intelligent control, and renewable-energy systems. He is a student member of SICE and ACA.

Kenko Uchida received the B.S., M.S. and Dr.Eng. degrees of Electrical Engineering from Waseda University, Japan in 1971, 1973 and 1976, respectively. He is currently a Professor in the Department of Electrical Engineering and Bioscience, Waseda University. His research interests are in robust/optimization control and control problem in energy systems and biology. He is a member of SICE, ACA, IEEJ, and IEEE.